ISSN 1674-1056
http://cpb.iphy.ac.cn
http://iopscience.iop.org/cpb
中国物理 B
Chinese Physics
中国物理 Chinese Physics B

Effect of microstructure on ^{3}He migration in $TiT_{1.9}$ films

Haifeng Wang(王海峰), Shuming Peng(彭述明), Wei Ding(丁伟), Huahai Shen(申华海), Weidu Wang(王维笃), Xiaosong Zhou(周晓松), Xinggui Long(龙兴贵)

Citation: Chin. Phys. B . 2018, 27(9): 096103. **doi:** 10.1088/1674-1056/27/9/096103

Journal homepage: http://cpb.iphy.ac.cn; http://iopscience.iop.org/cpb

What follows is a list of articles you may be interested in

Material microstructures analyzed by using gray level Co-occurrence matrices

Yansu Hu(胡延苏), Zhijun Wang(王志军), Xiaoguang Fan(樊晓光), Junjie Li(李俊杰), Ang Gao(高昂)

Chin. Phys. B . 2017, 26(9): 098104. **doi:** 10.1088/1674-1056/26/9/098104

Interface states study of intrinsic amorphous silicon for crystalline silicon surface passivation in HIT solar cell

You-Peng Xiao(肖友鹏), Xiu-Qin Wei(魏秀琴), Lang Zhou(周浪)

Chin. Phys. B . 2017, 26(4): 048104. **doi:** 10.1088/1674-1056/26/4/048104

Microstructure evolution of Cu atomic islands on liquid surfaces in the ambient atmosphere

Zhang Xiao-Fei, Chen Hang, Yu Sen-Jiang

Chin. Phys. B . 2015, 24(7): 076103. **doi:** 10.1088/1674-1056/24/7/076103

Room temperature damping correlated to the microstructures in Cu-20.4Al-8.7Mn

Hao Gang-Ling, Wang Xin-Fu, Wang Hui, Li Xian-Yu

Chin. Phys. B . 2015, 24(6): 066104. **doi:** 10.1088/1674-1056/24/6/066104

Superior tribological properties of an amorphous carbon film with a graphite-like structure

Wang Yong-Jun, Li Hong-Xuan, Ji Li, Liu Xiao-Hong, Wu Yan-Xia, Zhou Hui-Di, Chen Jian-Min

Chin. Phys. B . 2012, 21(1): 016101. **doi:** 10.1088/1674-1056/21/1/016101

Effect of microstructure on ^{3}He migration in $TiT_{1.9}$ films

Haifeng Wang(王海峰), Shuming Peng(彭述明)†, Wei Ding(丁伟), Huahai Shen(申华海), Weidu Wang(王维笃), Xiaosong Zhou(周晓松), and Xinggui Long(龙兴贵)

Institute of Nuclear Physics and Chemistry, China Academy of Engineering Physics, Mianyang 621900, *China*

(Received 11 March 2018; revised manuscript received 27 May 2018; published online 28 August 2018)

Two kinds of films were prepared to study the effect of microstructure on helium migration in Ti tritides. Both films showed different release behaviors and helium bubble distributions. In the film consisting of columnar grains, a two-layered structure was observed. Inclusions with a strip feature were found at the grain boundary, and no helium bubbles were distributed in these inclusions. However, helium preferred to migrate to the boundaries of these inclusions. Bubble linkage as a ribbon-like feature developed parallel to the film surface in the film consisting of columnar grains. More cracks were developed at the grain boundaries of the film consisting of columnar grains, although the helium content in the film consisting of columnar grains was less than that in the film consisting of equiaxed grains. A surface region with a small number of bubbles, or "depleted zone", was observed near the surface. The cracks extending to the film surface were the pathways of the critical helium released from the film. The helium migration was strongly influenced by the grain microstructure.

Keywords: helium bubble, Ti tritide, microstructure

PACS: 61.72.Qq, 81.40.Wx, 68.55.–a **DOI:** 10.1088/1674-1056/27/9/096103

1. Introduction

Tritium has many important technological applications. It is common to combine tritium with a metal to form metal tritides for stable, high-density storage of tritium. ^{3}He is produced by the radioactive decay of tritium. It is well known that at least initially, most of the ^{3}He remains in the solid, and only less than 1% of the generated ^{3}He is released from metal tritides.[1,2] Snow *et al.* showed that the total amount of helium released early in life was independent of the film thickness, which suggested that the helium released early in life came from the near-surface region.[3] When the helium concentration in metal tritides reached a critical value, helium was released at rates equal to or sometimes exceeding the generation rate. The onset of critical release was found to vary for different metals, and it occurred around 0.3 (He:metal ratio) for erbium tritides and titanium tritides, and around 0.40 for zirconium tritides.[2] Helium accumulation in metal tritides would cause considerable changes in the structure and properties of these materials, such as volume expansion and the decrease of the plateau pressure.

The recoil energy of ^{3}He created by tritium decay was estimated to be ~ 1.03 eV, which was too low to make it leave the tetrahedral site in which it was created.[4] It was found that helium atoms could become weakly bound to either lattice defects or other helium atoms they encountered as they migrated.[5,6] It has also been proved that the interstitial helium can strongly bind to the grain boundary.[7] Helium bubbles in aging metal tritides were commonly seen in the lattice and grain boundary by the transmission electronic microscopy (TEM).[8–12] Helium bubble evolution in metal tritides is a complicated process, the study of which requires modeling at many different levels including atomic properties of ^{3}He atoms in metal lattices, diffusion mechanisms, kinetics of bubble nucleation and growth, and the relationship between the microstructural evolution and the change in mechanical properties.[13,14]

The microstructure of the film was believed to have a strong effect on the helium migration and has been studied extensively.[3,15–18] The structure of films could involve a number of characteristics, such as grain size, strain, crystallographic orientation, and so on. It was shown that the film structure was strongly affected by the preparation procedures and deposition condition, such as substrate temperature,[19,20] deposition rate,[21] substrate materials,[22] impurity contamination, and film thickness.[23–25]

The purpose of this paper is to study ^{3}He migration in $TiT_{1.9}$ films. We prepared two kinds of Ti tritide films with different grain morphologies, and presented the results of the helium release measurement and TEM analysis of these two kinds of Ti tritide films during aging. The decisive factors in microstructure and the roles of these factors on the helium bubble distribution and helium release were clarified.

2. Experimental procedures

2.1. Film growth and tritium loading

In this study, two kinds of titanium films were prepared to several micrometers by physical evaporation on rolled molybdenum substrates. The film of sample C was deposited at a rate of 25 nm/s by electron-beam evaporation, and the film of

†Corresponding author. E-mail: pengshuming@caep.cn

© 2018 Chinese Physical Society and IOP Publishing Ltd

sample E was deposited at a rate of 100 nm/s by resistance heating. The substrate temperature was 500 °C, and the pressure of the vacuum system was 2×10^{-4} Pa for all the samples during evaporation. The thicknesses of these films were almost the same by controlling the deposition time.

These films were transported to a tritiding facility and loaded with tritium to produce tritide films with the initial composition of $TiT_{1.9}$. The amount of the absorbed tritium in films was estimated by deducting the exact residual pressure from the initial loading tritium pressure in the container. The samples were stored in a vacuum vessel at room temperature, and the amount of helium released during the storage was measured by a quadrupole mass spectrometer (QMS). The ^{3}He concentration in the aging samples was obtained from both the initial tritium content and the aging time, which was revised by the releasing amount of helium from the film surface.

2.2. TEM preparation and analysis

The cross-sectional TEM samples were obtained using a focused-ion beam instrument (FIB). From the titanium tritide films, 20 μm×10 μm sections were cut and mounted on FIB half grid. The samples were then thinned to ∼ 100 nm by FIB. During these processes, helium may be released from the surface layer, and the surface layers may be amorphized by ion milling. In addition to inclining the incident ion beam to the surface of the specimen and lowering the beam energy to minimize these effects, more thick films were preserved to retain the physical environment for helium only when it did not influence the observation in the TEM. The prepared samples were transferred from FIB to TEM in several minutes. TEM analysis was performed using an FEI F30 300 kV TEM.

3. Results

A large number of measurements have been made on helium emission from these two kinds of Ti tritide films in the past.[2] Figure 1 shows the normalized ^{3}He release rate fraction (release rate/generation rate) from these two kinds of films as a function of the generated ^{3}He concentration. Helium release can be divided into two regions: an "early release" period characterized by a constant and small release fraction, and a "critical release" period where the helium is released at rates equal to and sometimes exceeding the generation rate.[1] The onset of the critical release occurs below 0.28 (He:Ti ratio) for sample C and around 0.3 or more for sample E. The early release fraction of Ti tritides is similar to that of Zr tritides, but lower than Er tritides by more than one order of magnitude.[2]

The crystal structures of these two kinds of films were studied by x-ray diffraction (XRD), and the results are shown in Fig. 2. The peak broadening and overlap with the peaks of the Mo substrate make it difficult to find the differences. There are both (110) out of plane and (200) out of plane rolling texture in our Mo substrate. Because the {110} and {200} spacing for Mo is close to the {200} and {220} spacing for $TiH_{1.9}$, respectively, these $TiT_{1.9}$ films show both (200) out of plane and (220) out of plane textures.[26] More studies will be carried out in the future on the pole figure for these two kinds of films.

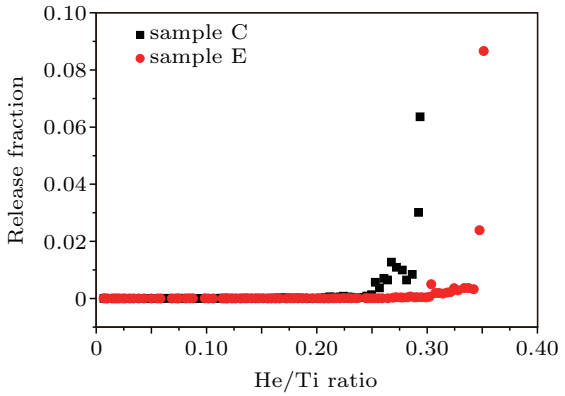


Fig. 1. (color online) Normalized He release rate from Ti tritide samples as a function of the generated He concentration.

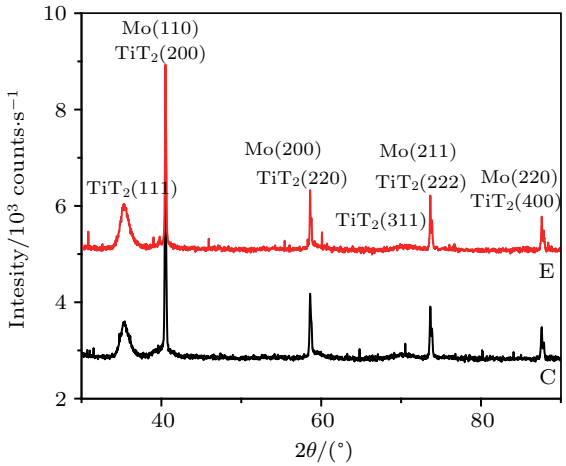


Fig. 2. (color online) Diffraction peaks of the two kinds of films. He:Ti ratios of sample C and E are 0.299 and 0.356, respectively.

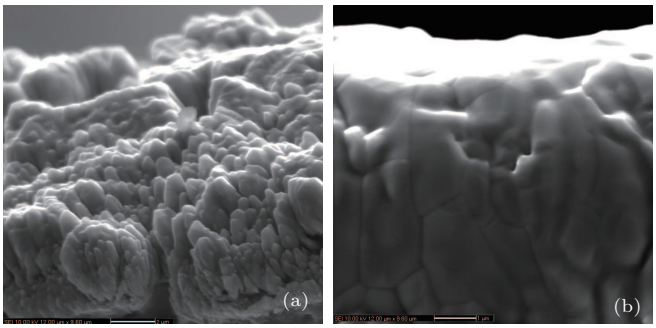


Fig. 3. Cross-sections of the two kinds of films before tritiation. (a) Columnar grain structure of sample C. (b) Equiaxed grain structure of sample E.

Figures 3 and 4 show the grain structures of the two kinds of films before and after tritiation. Obviously the process of hydriding does not change the microstructure of the

two kinds of films. The cross-section of sample C shows a multi-layered columnar grain structure. The upper layer is obviously made up of stacked flaky crystals perpendicular to the surface. Savaloni *et al.* studied the growth of erbium films on Mo substrates with different roughness, different substrate temperatures, different deposition rates, and under three different ultra-high vacuum (UHV) conditions, namely standard, semi-rigorous, and rigorous.[27] They observed that for substrate temperatures up to 775 K, all the films produced under the rigorous UHV condition, in contrast to those produced under the standard UHV condition, were free from growth steps and layering. The growth steps and the corresponding layered cross-section were the results of film oxidation, which was due to the poor vacuum condition. The decreased mobility of contaminated grain boundaries limited further grain growth.

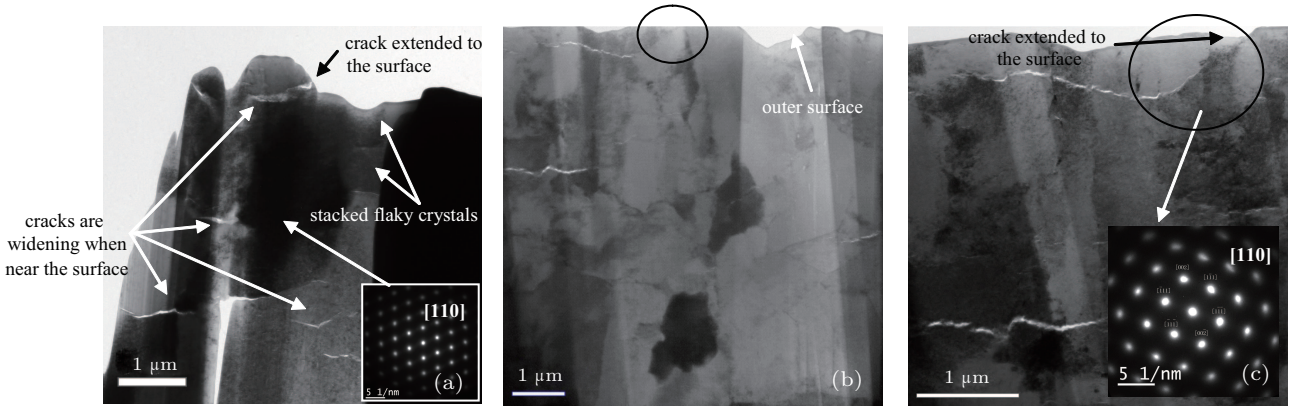


Fig. 4. Grain structure and ^{3}He-filled cracks in the two kinds of films at the beginning of accelerated release. (a) Columnar grain structure of sample C at He:Ti ratio of 0.299. (b)–(c) Equiaxed grain structure of sample E at He:Ti ratio of 0.356. The circled areas in (b) and (c) show the hidden right part of the crack which is growing along one of the {111} planes of the grain below as indicated by the corresponding selected-area diffraction pattern (close to [110] zone axis).

The grain in sample E is a typical equiaxed three-dimensional structure. The film of sample E was deposited at a high deposition rate by resistive heating, and the grains grew faster, thereby favoring grain coarsening and restructuration, as well as less oxygen contamination.

Figure 4 shows that cracks are developed along the grain boundary of both samples at the beginning of the helium accelerated release stage. Most of these cracks are nearly parallel to the film surface. Almost all these cracks occur in regions of grain boundary where the boundary is approximately parallel to one of the equivalent sets of {111} planes in at least one of the adjacent grains. This can be confirmed by the appearance of the hidden part of the crack near the film surface when the sample is tilted to allow the {111} planes of the grain below to become parallel to the electron beam, as shown in Figs. 4(b) and 4(c).

More cracks are found in sample C, and these cracks become wider as they approach the film surface, as shown in Fig. 4(a). The cracks in sample E are few and narrow. It can be observed that in both samples, cracks extend to the film surface. The sudden connection of such cracks to the outside may bring about large bursts of ^{3}He into the atmosphere.

The helium content of sample C is lower than that of sample E, but more cracks developed in sample C, which implies that there are more helium atoms migrating from the interior grain to the grain boundary in sample C than in sample E.

Figure 5 illustrates the helium bubble distribution in the grains of these two kinds of films. Compared with sample E, sample C shows a strong bubble linkage and orientation distribution. Many bubbles congregate as ribbon-like features in Fig. 5(a). Nearly all these ribbon-like features are parallel to the film surface. Some helium bubbles are aggregated as loops in sample C. The sizes of these loops are less than 5 nm. Large loops tend to transform into a ribbonlike structure. The bubbles aggregated as loops are more commonly seen on the thin fringe of the samples with low helium content because of the stress release in these regions. Accordingly, there may be stress release in the grains of sample C. In sample E, many interconnected bubble strings are observed in a uniform distribution in the grains.

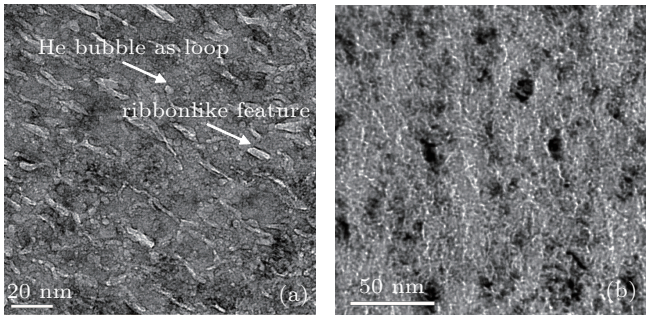


Fig. 5. Helium bubble distribution inside grains of the two kinds of films. (a) Sample C at He:Ti ratio of 0.299. (b) Sample E at He:Ti ratio of 0.356.

Figure 6(a) shows the crack along the grain boundaries in sample C. These cracks develop along a strip feature at the grain boundary. The strip features can be found in the grain or

boundaries of both kinds of films. Figure 6(b) shows the strip feature distributed in the grain of sample E. Similar inclusions were also found in almost all Er tritide samples, which was confirmed to be oxide particles.[3] One possibility is that the strip feature is formed by the enrichment of oxygen on the grain surface when preparing the film. No helium bubble is distributed in these strip features while a high concentration of helium is distributed at the boundaries of these inclusions.

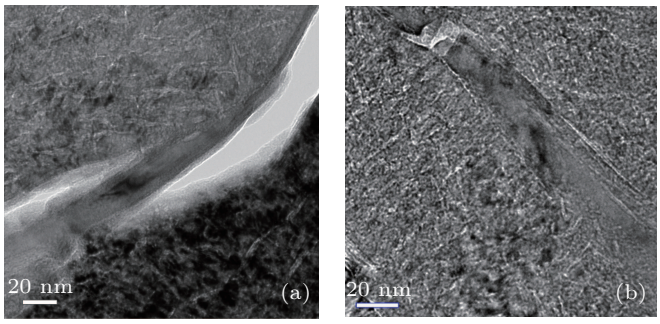


Fig. 6. (a) A big crack along the strip feature at the grain boundaries of sample C. (b) The strip feature distributed in the grain of sample E.

Figure 7 shows that a few helium bubbles are observed near the surface region and many large-size black loops have developed near the surface. These tiny bubbles distributed near the surface are dispersed compared with the interconnected bubbles in the inner films. This zone termed a "denuded zone" or "depleted zone" has been reported in other materials.[28–30] The thickness of the depleted zone is $\sim$ 25 nm. The origin of this region can be understood by assuming that most of the helium created in this region diffuses to the surface and thus the bubble density is reduced.[31,32] Snow *et al.* observed $\sim$ 15 nm of surface region void of helium bubbles in $Er(D,T)_2$ films.[3] Their samples were not at the helium accelerated release stage, and no such loops were observed in $Er(D,T)_2$ films.

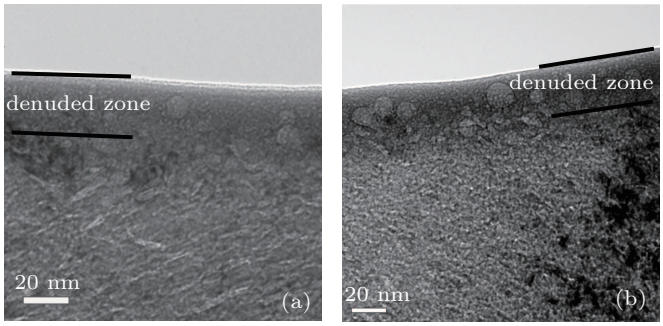


Fig. 7. Helium bubble distribution near the film surface. (a) Sample C at He:Ti ratio of 0.299. (b) Sample E at He:Ti ratio of 0.356.

As the helium content in the film increases, the stress increases, which would result in a large difference in stress between the inner films and the surface. These loops are likely to be produced by the high internal stress. The number and the size of these loops in sample E are higher than those in sample C. The increase of the stress with helium content in the samples would generate more dislocations in the surface layer and drive the growth of these dislocations.

4. Discussion

The film structure of sample C is a multi-layered columnar grain. In the model of Barna *et al.*, the formation of polycrystalline films is considered as the growth of many single crystallites through the growth of characteristic layers, which occurs on their individual crystallographic faces.[33] The presence of foreign atoms or molecules directly influences these processes. The adsorbed oxygen continuously accumulates at growth steps. Consequently, two-dimensional oxide films are formed, obstructing layer growth.[21] This can be confirmed by the strip inclusion distributed on the boundaries of two-layered columnar grains, as shown in Fig. 6(a). Sample C was prepared at a low deposition rate. Therefore, more oxygen was introduced during the film growth. The layer growth was then seriously interrupted, and finally a stacked flaky crystal was generated. The crack at grain boundaries in sample C broadens when it is close to the surface, indicating the low interfacial energy between the grains. The weak binding energy or the high density of foreign atoms or molecules at the boundary between these mismatched grains accelerates the migration of the surrounding helium atoms to the boundaries and the development of cracks.

Inclusions are generally observed in all Ti tritide samples. Some of them are distributed inside grains, but most of them are distributed at grain boundaries. The inclusions in Ti tritides appear as long strips, which are different from the particle-shaped oxides in $Er(D,T)_{2-x}{}^3He_x$.[3] The energy-dispersive x-ray spectroscopy (EDS) analyses of these inclusions did not show the signal of oxygen. Parish *et al.* studied the oxygen contamination in ErD_2 thin films and indicated that due to oxygen's low x-ray and the easy absorption of soft oxygen x-rays, EDS was not expected to yield high signal-to-noise ratios for oxygen.[16] However, energy-filtered TEM showed thick near-surface oxides and intrafilm oxide particles in the D-loaded ErD_2 films.[16] Thus the strip feature in Ti tritide films is probably flaky and has a low oxygen distribution.

Snow *et al.* studied helium release in $Er(D,T)_{2-x}{}^3He_x$ films and showed that the amount of helium released as a function of film thickness was relatively constant, suggesting that helium was being released only from the near-surface region and did not diffuse into the surface from the interior of the film.[3] The surface of Ti tritide films forms a thicker depleted zone than Er tritides, but the early release fraction for Ti tritides is lower by more than one order of magnitude.[2] There are more bubbles observed in the depleted zone of the Ti tritide films. Accordingly, the difference of helium diffusion rate in the depleted zone of the Ti and Er tritide films is obvious.

The slow helium diffusion rate in the depleted zone of the Ti tritide films could be responsible for the observation of more helium bubbles and the low early release fraction from the film surface.

Compared with sample E, sample C shows strong helium bubble linkage and orientation distribution in the grains. The bubble coalescence in the grains is probably the result of the stress distribution in the film. Rodriguez *et al.* made a detailed XRD analysis of the ErT_2 film, which revealed significant in-plane compressive macro-strain due to ^{3}He bubble formation/growth.[34] The different size and number of dislocation loops ejected on these two kinds of film surfaces could be understood by the different stress distributions in these two films. It seems that a higher stress is distributed in sample E and relatively low stress is distributed in sample C.

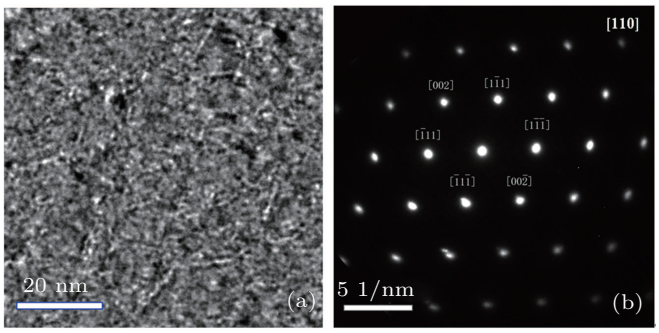


Fig. 8. Bright-field images of samples at He:Ti ratios of 0.109. (a) Underfocus; (b) the corresponding diffraction pattern of the selected-area (close to [110] zone axis).

Before the bubble interconnection, it is common to observe helium bubbles distributed along {111} planes, as shown in Fig. 8, after which in sample C almost all of these bubbles are linked as a ribbon-like feature parallel to the film surface. However, few bubbles are linked perpendicular to the film surface, as shown in Fig. 5(a). Many metal tritides showed a steady expansion rate during their storage since the ^{3}He atoms required more space than the tritium atoms.[35–37] Obviously, the film swelling would release the stress perpendicular to the film surface to a certain extent, which may impede the bubble interconnection in that direction. Helium bubbles tended to distribute with the orientation of high stress. The crack widening near the surface can also be understood by the film swelling in sample C.

At He/Ti = 0.27, the He release rate for sample E begins to increase rapidly from a constant value, much later than sample C in Fig. 1. The rapid increase of He release rate has been widely seen in Ti, Zr, and Er tritides when the sample is coming in the critical release period. Obviously this change comes from the depleted zone of the film surface. The interconnected bubbles beneath the depleted zone (Fig. 7) may not contribute to the critical release of helium. Mitchell *et al.* observed that the ^{3}He release rate from erbium and zirconium ditritide films exhibited some differences and appeared to be associated with the spontaneous release of helium in bursts of about 10^9 atoms.[38] This irregular ^{3}He release should only come from the cracks extending to the film surface.

5. Conclusion

The helium migration is greatly affected by the grain structure of the film. The migration and accumulation of helium at the grain boundary would be accelerated in the film consisting of columnar grains due to its small flaky grain structure and grain orientation distribution, compared with the film consisting of equiaxed grain structure. Columnar grains are weakly bonded and easily separated by the accumulation of helium on the grain boundaries. Cracks develop along the grain boundary in both films, most of which are nearly parallel to the film surface and widen near the surface. Bubble linkage as a ribbonlike feature develops parallel to the film surface in the film consisting of columnar grains. Inclusions as a strip feature are found in both kinds of films, at the boundary of which a high concentration of helium is observed. The critical ^{3}He release from the surface comes from the cracks developed at grain boundaries extending to the film surface.

Acknowledgments

Helpful discussions with W P Cai, M Chen, and G J Chen are acknowledged. The authors would like to thank H H Shen for the help in performing the experiment.

References

[1] Beavis L C and Kass W J 1977 *J. Vac. Sci. Technol.* **14** 509
[2] Ding W, Long X G and Liang J H 2008 *At. Engergy Sci. Technol* **42** 944 (in Chinese)
[3] Snow C S, Brewer L N, Gelles D S, Rodrguez M A, Kotula P G, Banks J C, Mangan M A and Browning J F 2008 *J. Nucl. Mater.* **374** 147
[4] Chen R C, Yang L and Dai Y Y 2012 *Chin. Phys. B* **21** 056601
[5] Zu X T, Yang L, Gao F, Peng S M, Heinisch H L, Long X G and Kurtz R J 2009 *Phys. Rev. B* **80** 054104
[6] Zhang B L, Wang J and Hou Q 2011 *Chin. Phys. B* **20** 036105
[7] Gong H F, Yan Y, Zhang X S, Lv W, Liu T and Ren Q S 2017 *Chin. Phys. B* **26** 093104
[8] Thiébaut S, Décamps B, Pénisson J M, Limacher B, and Guégan A Percheron 2000 *J. Nucl. Mater.* **277** 217
[9] Schober T, Trinkaus H and Lässer R 1986 *J. Nucl. Mater.* **141** 453
[10] Bond G M, Browning J F and Snow C S 2010 *J. Appl. Phys.* **107** 083514
[11] Snow C S, Browning J F, Bond G M, Rodriguez M A and Knapp J A 2014 *J. Nucl. Mater.* **453** 296
[12] Trinkaus H and Singh B N 2003 *J. Nucl. Mater.* **323** 229
[13] Gao X, Luo P and Chang H L 2015 *Chin. Phys. Lett.* **32** 76101
[14] Chen M 2011 *Acta Phys. Sin.* **60** 126602 (in Chinese)
[15] Parish C M, Snow C S, Kammler D R and Brewer L N 2010 *J. Nucl. Mat.* **403** 191
[16] Parish C M, Snow C S, and Brewer L N 2009 *J. Mater. Res.* **24** 1868
[17] Liang L, Tan X H, Xiang W, Wang Y, Cheng Y L and Ma M W 2015 *Acta Phys. Sin.* **64** 046103 (in Chinese)
[18] Zhou Y L, Deng A H, Li R S, Zhang B L and Hou Q 2011 *Acta Phys. Sin.* **60** 046604 (in Chinese)
[19] Shen H H, Peng S M, Long X G, Zhou X S, Yang L, Liu J H, Sun Q Q and Zu X T 2012 *Chin. Phys. B* **21** 076101

[20] Shen H H, Peng S M, Long X G, Zhou X S, Yang L and Zu X T 2012 *Vacuum* **86** 1097
[21] Savaloni H, Player M A, Gu E and Marr G V 1992 *Vacuum* **43** 965
[22] Peng S M, Shen H H, Long X G, Zhou X S, Yang L and Zu X T 2012 *Acta Phys. Sin.* **61** 176106
[23] Shen H H, Zu H Y, Peng S M, Yang L, Zhou X S, Sun K, Xiang X and Zu X T 2013 *Mater. Lett.* **106** 259
[24] Savaloni H, Taherizadeh A and Zendehnam A 2004 *Physica B* **349** 44
[25] Guo D C, Jiang X D, Huang J, Wang F R, Liu H J, Xiang X, Yang G X, Zheng W G and Zu X T 2014 *Opt. Express* **22** 29020
[26] Zhou X S, Long, X G and Peng S M 2010 *J.Nucl.Mater.* **396** 223
[27] Savaloni H and Player M A 1995 *Vacuum* **46** 167
[28] Trinkaus H 1986 *Radiat. Eff.* **101** 91
[29] Schober T and Farrell K 1989 *J. Nucl. Mater.* **168** 171
[30] Schroeder H 1989 *J. Nucl. Mater.* **155–157** 1032
[31] Chen J, Hung P and Trinkaus H 2000 *Phys. Rev. B* **61** 12923
[32] Singh B N, Leffers T and Green W V 1984 *J. Nucl. Mater.* **125** 287
[33] Grobenor C R M, Hentzell H T G and Smith D A 1984 *Acta Metall.* **32** 773
[34] Rodriguez M A, Browning J F and Frazer C S 2007 *Powder Diffr.* **22** 118
[35] Beavis L C and Miglionico C J 1972 *J. Less-Common Met.* **27** 201
[36] Schober T and Trinkaus H 1991 *J. Appl. Phys.* **70** 729
[37] Schober T and Trinkaus H 1990 *J. Appl. Phys.* **67** 7587
[38] Mitchell D J and Provo J L 1985 *J. Appl. Phys.* **57** 1855